Sea surface pCO_2 and O_2 in the Southern Ocean during the austral fall, 2008

T. S. Moore,[1] M. D. DeGrandpre,[1] C. L. Sabine,[2] R. C. Hamme,[3] C. J. Zappa,[4] W. R. McGillis,[5] R. A. Feely,[3] and W. M. Drennan[6]

Received 29 July 2010; revised 8 August 2011; accepted 7 September 2011; published 16 November 2011.

[1] The physical and biological processes controlling surface mixed layer pCO_2 and O_2 were evaluated using in situ sensors mounted on a Lagrangian drifter deployed in the Atlantic sector of the Southern Ocean (~50°S, ~37°W) during the austral fall of 2008. The drifter was deployed three times during different phases of the study. The surface ocean pCO_2 was always less than atmospheric pCO_2 (−50.4 to −76.1 μatm), and the ocean was a net sink for CO_2 with fluxes averaging between 16.2 and 17.8 mmol C m^{-2} d^{-1}. Vertical entrainment was the dominant process controlling mixed layer CO_2, with fluxes that were 1.8 to 2.2 times greater than the gas exchange fluxes during the first two drifter deployments, and was 1.7 times greater during the third deployment. In contrast, during the first two deployments the surface mixed layer was always a source of O_2 to the atmosphere, and air-sea gas exchange was the dominant process occurring, with fluxes that were 2.0 to 4.1 times greater than the vertical entrainment flux. During the third deployment O_2 was near saturation the entire deployment and was a small source of O_2 to the atmosphere. Net community production (NCP) was low during this study, with mean fluxes of 3.2 to 6.4 mmol C m^{-2} d^{-1} during the first deployment and nondetectable (within uncertainty) in the third. During the second deployment the NCP was not separable from lateral advection. Overall, this study indicates that in the early fall the area is a significant sink for atmospheric CO_2.

Citation: Moore, T. S., M. D. DeGrandpre, C. L. Sabine, R. C. Hamme, C. J. Zappa, W. R. McGillis, R. A. Feely, and W. M. Drennan (2011), Sea surface pCO_2 and O_2 in the Southern Ocean during the austral fall, 2008, *J. Geophys. Res.*, *116*, C00F11, doi:10.1029/2010JC006560.

1. Introduction

[2] The Southern Ocean, which makes up 10% of the world's oceans, is thought to be responsible for 9%–40% of the oceanic uptake of anthropogenic CO_2 [*Sabine et al.*, 2004; *Fletcher et al.*, 2006; *Khatiwala et al.*, 2009], removing 0.06 to 0.4 Pg C yr^{-1} from the atmosphere [*McNeil et al.*, 2007; *Takahashi et al.*, 2009]. The wintertime partial pressure of CO_2 (pCO_2) in the Southern Ocean (50°S–60°S) was increasing at a mean rate of 2.1 ± 0.6 μatm yr^{-1} between 1981 and 2008 [*Takahashi et al.*, 2009], somewhat faster than the global mean atmospheric pCO_2 increase of 1.7 ± 0.1 μatm yr^{-1} [*Le Quéré et al.*, 2010; P. Tans, http://www.esrl.noaa.gov/gmd/ccgg/trends/, 2009] over the same time period. Historically the Southern Ocean has been undersampled; however, recognition of its importance in the global carbon cycle has resulted in it receiving considerable attention from the scientific community in recent years.

[3] The Southern Ocean, and in particular the area encompassed by the Antarctic Circumpolar Current (ACC), is known for its strong westerly winds (the "Roaring Forties"). Climate models of the Southern Ocean find that wind speed will increase with global warming [*Fyfe and Saenko*, 2005; *Zickfeld et al.*, 2007; *Lovenduski et al.*, 2008], which will increase rates of air-sea gas transfer. The models have also found that the increase in wind speed will also increase Ekman transport, and consequently upwelling of carbon- and nutrient-rich deep waters in the southern ACC and downwelling in the northern ACC [*Hall and Visbeck*, 2002; *Bryden and Cunningham*, 2003; *Marshall*, 2003; *Oke and England*, 2004]. However, the magnitude of these changes remains uncertain [e.g., *Lenton and Matear*, 2007; *Boning et al.*, 2008; *Saenko*, 2008]. The Southern Ocean is also a high-nutrient, low-chlorophyll region, with biological productivity

[1]Department of Chemistry and Biochemistry, University of Montana, Missoula, Montana, USA.
[2]Pacific Marine Environmental Laboratory, Seattle, Washington, USA.
[3]School of Earth and Ocean Sciences, University of Victoria, Victoria, British Columbia, Canada.
[4]Ocean and Climate Physics Division, Lamont-Doherty Earth Observatory, Earth Institute at Columbia University, Palisades, New York, USA.
[5]Earth and Environmental Engineering, Lamont-Doherty Earth Observatory, Earth Institute at Columbia University, New York, New York, USA.
[6]Rosenstiel School of Marine and Atmospheric Science, University of Miami, Miami, Florida, USA.

Copyright 2011 by the American Geophysical Union.
0148-0227/11/2010JC006560

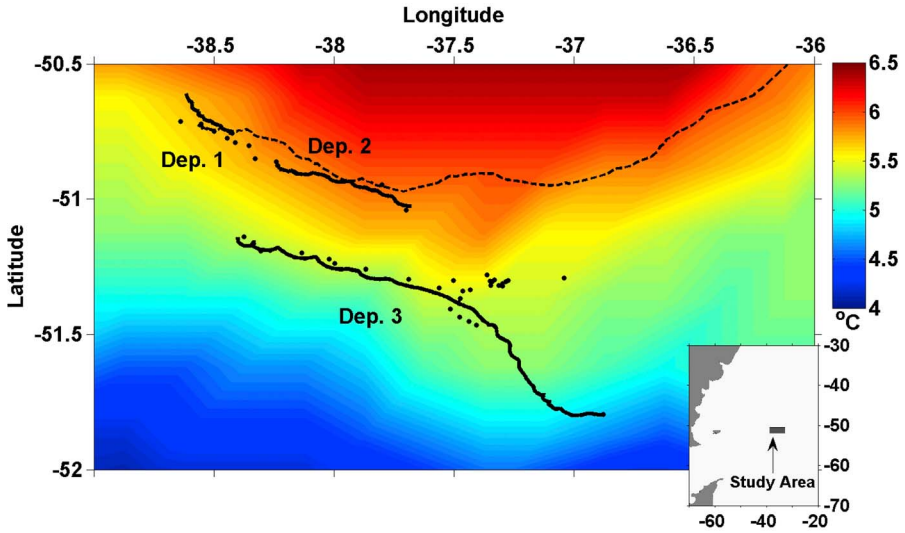

Figure 1. Deployment locations of the $MAPCO_2$ (solid line) and ASIS drifters (dashed line) and CTD cast sites (dots) overlain on a map of satellite-derived SST for 18 March (TMI and AMSR-E satellites). The $MAPCO_2$ drifter was deployed three times, twice in the initial tracer patch (northwest deployments) and once in the second tracer patch (southern deployment). The line for the first $MAPCO_2$ deployment is short and partially obscured by the CTD markers and the line for the ASIS data. The CTD cast sites indicate the central location of the tracer patches.

being primarily Fe limited [*Martin et al.*, 1990; *de Baar et al.*, 1999]. Observed rates of productivity range from −11 to +240 mmol C m^{-2} d^{-1} [*Quéguiner et al.*, 1997; *Boyd et al.*, 2000; *Gervais et al.*, 2002; *Strass et al.*, 2002; *Coale et al.*, 2004; *Fransson et al.*, 2004a; *Shim et al.*, 2006; *Guéguen and Tortell*, 2008; R. C. Hamme et al., Unusual productivity dynamics in the Southern Ocean: Following the SO GasEx Lagrangian tracer patches, submitted to *Journal of Geophysical Research*, 2011] based on a wide variety of methods used (^{14}C, $\Delta O_2/Ar$, and O_2, NO_3^-, and C mass balance). Seasonal blooms can lead to significant CO_2 undersaturation, with observed pCO_2 as much as 180 μatm below atmospheric levels [e.g., *Guéguen and Tortell*, 2008]. Increased upwelling of nutrient-rich waters will stimulate primary productivity, drawing down pCO_2 in the surface waters, thereby potentially enhancing the uptake of anthropogenic CO_2. However, upwelled waters also have elevated pCO_2, which will decrease the net air-sea CO_2 uptake.

[4] While limited in terms of mapping biogeochemical provinces, Lagrangian studies in other regions have observed the natural CO_2 cycle in individual water masses. Lagrangian studies in the eastern equatorial Pacific Ocean [*DeGrandpre et al.*, 2004] found that diel heating, followed by net community production (NCP) and air-sea gas exchange were responsible for the observed diel changes in mixed layer pCO_2. Lagrangian studies in the Greenland Sea [*Hood et al.*, 1999] found that NCP drew down surface CO_2 concentrations in the summer, and that this draw down was offset by vertical entrainment of CO_2 rich waters, gas exchange, and respiration. Lagrangian studies in the North Atlantic [*Hood et al.*, 2001; *Merlivat et al.*, 2009] and the equatorial Atlantic [*Bakker et al.*, 2001] have observed the effects of storms, biological productivity, and seasonal upwelling processes.

[5] Studies on individual water masses in the Southern Ocean have primarily been part of iron fertilization experiments and air-sea gas exchange studies [*Boyd et al.*, 2000; *Gervais et al.*, 2002; *Coale et al.*, 2004]. During these studies unaltered waters had primary productivity rates of 11–17 mmol C m^{-2} d^{-1}, which increased up to 64–276 mmol C m^{-2} d^{-1} with the addition of Fe, resulting in a 20–40 μatm drawdown in pCO_2. To our knowledge, the only other Lagrangian drifter study of pCO_2 was performed in the Pacific sector of the Southern Ocean in 2004–2005 using CARIOCA drifters [*Barbero et al.*, 2011].

[6] In March 2008, we deployed a Lagrangian drifter as part of the Southern Ocean Gas Exchange cruise (SO-GasEx) to investigate carbon cycling within an individual water mass in the Southern Ocean under high wind speeds and long fetch waves. The drifter provided high-frequency measurements (every 1/2 h) of pCO_2, dissolved oxygen (O_2), and temperature at multiple depths in the upper 100 m of the water column. These data were used to calculate air-sea gas exchange and vertical entrainment fluxes for CO_2 and O_2, and the results were used in a 1-D mass balance of dissolved inorganic carbon (DIC) and O_2. This study provides an important assessment of the types of processes controlling the mixed layer pCO_2, dissolved inorganic carbon, and dissolved oxygen in the Southern Ocean.

2. Study Site and Methods

2.1. Study Site

[7] The SO-GasEx cruise took place in the southern Atlantic Ocean south of the Polar Front (PF). Antarctic Intermediate Water (AAIW) forms in this region, as denser waters from the south sink below less dense waters from the north [*Bakker et al.*, 1997; *Olbers and Visbeck*, 2005]. The $MAPCO_2$ drifter (see below) was deployed at 50°35′S, 38°40′W (Figure 1) on 8 March 2008 by the R/V *Ronald H. Brown* on the south side of an eddy, after injection of

a $^3He/SF_6$ tracer patch at the site. An ASIS drifter (described below) was deployed in the patch on 10 March 2008 (Figure 1). During the SO-GasEx cruise $^3He/SF_6$ concentrations, monitored along ship transects, were used to calculate air-sea gas fluxes and to confirm that the drifters were Lagrangian; for details on the tracer patch see *Ho et al.* [2011a]. During the first deployment the $MAPCO_2$ drifter was riding lower in the water than it was designed, and was recovered from the tracer patch on 12 March, reconfigured and redeployed on 13 March. Due to inclement weather and ship problems, the ship was forced to take refuge near South Georgia Island on 13 March while the $MAPCO_2$ and ASIS drifters remained in the water. On 17 March, the ship returned to the remnants of the first tracer patch (Figure 1), and the drifters were recovered on 18 March. The drogues on the mooring line were able to keep the $MAPCO_2$ drifter within the tracer patch. However, the ASIS drifter moved out of the tracer patch upon deployment (Figure 1). A new tracer patch was established at 51°9′S, 38°29′W and the $MAPCO_2$ drifter was redeployed on 21 March. The ASIS drifter was not redeployed. On 26 March, the $MAPCO_2$ drifter split from the main patch and drifted to the southeast (Figure 1). The drifter was recovered on 31 March within a portion of the tracer patch after it had drifted ~50 km from the main patch.

2.2. $MAPCO_2$ and ASIS Drifters

[8] The $MAPCO_2$ drifter contained an autonomous sensor that measures pCO_2 in the sea surface and atmosphere [*Friederich et al.*, 1995], 2 GPS tracking devices, and a SeaBird 37 Microcat sensor which recorded the temperature and conductivity at 1 m depth. Six 9 m "holey sock" drogues were mounted between 25 and 91 m depth. SAMI-CO_2 sensors [*DeGrandpre et al.*, 1995] (Sunburst Sensors) were mounted on a wire below the drifter at 5, 19, 34.5, 50, 75, and 105 m depth, sampling every 30 minutes. All SAMI-CO_2 sensors were equipped with oxygen optodes (Aanderaa Model 4175). No data were recovered from the 19 m SAMI-CO_2. Water temperature sensors (Onset PRO V2) were located below the drifter at 5, 19, 25, 34, 34.5, 40.5, 49.5, 50, 56, 65, 65.75, 74.75, 81.25, 90.25, 91, 100, and 105 m. After the first deployment the $MAPCO_2$ drifter was reconfigured to reduce the load, which included moving the 105 m SAMI-CO_2 up to 96 m, and removing the100 m and 105 m temperature sensors.

[9] The Air-Sea Interaction Spar (ASIS) drifter was designed to observe meteorological and wave conditions near the ocean surface [*Graber et al.*, 2000]. A SAMI-CO_2 sensor was mounted 1 m below the sea surface. Wind speed measured by the ASIS drifter was normalized to 10 m by converting the measured winds to neutral equivalent using the stability relationship of *Donelan* [1990], and then assuming a log layer profile to calculate the neutral wind speed at 10 m.

2.3. Shipboard Measurements

[10] The in situ data were compared to shipboard measurements for both data quality control and to aid interpretation. Underway pCO_2 measurements were performed on surface seawater collected from the bow intake (5 m depth) using an equilibrator infrared system [*Pierrot et al.*, 2009] calibrated with NOAA certified gas standards. As was noted by *Juranek et al.* [2010], the underway lines were cleaned with bleach prior to the cruise to prevent alteration of the CO_2 by respiration–underway/Niskin comparisons of dissolved O_2 showed that this treatment was successful. Underway pCO_2 data were postprocessed to in situ temperature and pressure. Every 12 h discrete samples were collected in the patch for dissolved inorganic carbon (DIC), total alkalinity (A_T), dissolved oxygen (O_2), and nutrients (NO_3^- [nitrate + nitrite], PO_4^{3-}, and silicic acid). Samples were collected at depths close to the depths of the SAMI-CO_2 sensors. DIC measurements were performed using the coulometric method [*Johnson et al.*, 1985], verified with certified reference materials (CRM, supplied by A. Dickson of Scripps Institution of Oceanography). After every 24 samples, 1–2 CRMS were run per CTD station, and the systems had an accuracy of 0.1 μmol kg^{-1} and a precision of ±0.33 μmol kg^{-1}. A_T measurements were performed using potentiometric titrations, and were verified by analyzing CRMs [*Dickson et al.*, 2003] every 24 samples. A_T measurements had an accuracy of 2 μmol kg^{-1} and a precision ±1 μmol kg^{-1}. Dissolved O_2 measurements were performed using Winkler titrations, and had a precision of ±0.15 μmol kg^{-1}. Nutrients were measured using an automated continuous flow system with segmented flow and colorimeteric detection [*Zhang*, 2000; *Zhang and Chi*, 2002]. Data were linearly interpolated with time and depth to match the sampling times and depths of the pCO_2 data.

2.4. Data Quality

[11] In situ data collected by the SAMI-CO_2 systems were compared with discrete and continuous shipboard measurements to ensure that the measurements were accurate. The 5 m SAMI-CO_2 had good agreement with the underway pCO_2 data once a 4 μatm offset was applied to the SAMI-CO_2 data. The SAMI-CO_2 data were within ±3–5 μatm of the pCO_2 calculated from the discrete A_T and DIC data using CO2SYS [*Pierrot et al.*, 2006] for data collected within the mixed layer, and were within ±5–10 μatm for data collected below the mixed layer. Although the SAMI response was not corrected for the effects of confining pressure at depth, the pressure dependence is negligible over this depth interval and did not contribute to the observed differences. In situ dissolved oxygen measurements were within 4 μmol kg^{-1} of the values measured by discrete Winkler titration (n = 41). During the start of the first drifter deployment the 5 m O_2 optode had a significant offset from the underway shipboard data, and during this time the underway O_2 data was used. Additionally, during the third drifter deployment the 5 m O_2 data differed from the underway O_2 data collected while the ship was near the drifter, however, the 35 m matched the underway data within uncertainty, and this data set was used for the mass balance calculations (see below). The differences between the in situ and discrete pCO_2 and O_2 measurements can be attributed at least in part to differences in water masses measured and the presence of an internal wave, which increased sampling uncertainty below the mixed layer.

2.5. Mass Balance and Flux Calculations

[12] We used a mass balance approach to compare the magnitudes of the different controlling processes, and to

identify periods when our understanding of the system is incomplete. A mass balance that incorporates the dominant processes controlling surface mixed layer inorganic carbon and dissolved oxygen concentrations is:

$$H\frac{dC}{dt} = F_{gasex} + F_{ent} - NCP, \quad (1)$$

where H is the surface mixed layer depth (H), $\frac{dC}{dt}$ is the rate of change of DIC or O_2 in the surface mixed layer, F_{gasex} is the air-sea gas exchange flux, F_{ent} is the vertical entrainment flux, and NCP is net community production (NCP = gross primary production − community respiration). All fluxes other than F_{gasex} were calculated using the average ML concentrations. F_{gasex} was calculated using the data from the 5 m sensors (except where noted above for Deployment 3), as this most closely reflects the air-water interface. There was no significant difference between the 5 m and average ML concentrations. In this Lagrangian experiment, we assume that the lateral advective flux is negligible; problems with this assumption are discussed in detail below. We assume that calcification was negligible based on the rates measured by *Balch et al.* [2011]. We are able to calculate F_{gasex} and F_{ent} as shown below, and NCP was calculated as the residual of equation (1). For all fluxes, a positive value indicates a flux into the surface mixed layer. A ratio of −106 DIC/141 O_2, determined by *Hiscock and Millero* [2005] during the SOFeX cruise, was used to convert NCP based upon O_2 into carbon units, and this NCP was compared to DIC-based NCP to evaluate the accuracy of the mass balance calculations. Our mass balance only focuses on changes within the surface mixed layer, and we do not address changes in the DIC and O_2 inventory below the mixed layer here.

[13] The O_2 mass balances were calculated using only the continuous, in situ data collected by the sensors on the $MAPCO_2$ drifter, with the exception noted above. In situ DIC concentrations for use in the DIC mass balance were calculated from the in situ pCO_2, pressure, temperature, salinity, and shipboard A_T and nutrients using CO2SYS [*Pierrot et al.*, 2006], and the *Mehrbach et al.* [1973] constants refit by *Dickson and Millero* [1987]. It should be noted that A_T and nutrient data were linearly interpolated to match the pCO_2 sampling frequency. The variability in A_T during the study was small, so we are confident that interpolation did not introduce significant uncertainty into our analyses. The modeled mixed layer pCO_2 was calculated based upon the mass balance of DIC and discrete A_T using the in situ temperature and pressure.

[14] Air-sea CO_2 gas fluxes were calculated using:

$$F_{gasex} = kS\Delta pCO_2, \quad (2)$$

where k is the gas transfer velocity calculated from the wind speed relationship determined during the SAGE cruise in the Southern Ocean [*Ho et al.*, 2006], S is solubility at in situ air pressure, temperature, and salinity [*Weiss*, 1974], and ΔpCO_2 is the difference between the pCO_2 in the atmosphere and the surface mixed layer (the mean atmospheric pCO_2 recorded by the $MAPCO_2$ sensor is 381 μatm). Air-sea gas fluxes for O_2 were calculated using:

$$F_{gasex} = k\Delta O_2, \quad (3)$$

where k is the gas transfer velocity calculated as above, using a Schmidt number for O_2 [*Wanninkhof*, 1992], ΔO_2 is the difference between O_2 saturation at atmospheric pressure [*Garcia and Gordon*, 1992], corrected for bubble entrainment [*Woolf and Thorpe*, 1991], and the observed O_2 concentration. Wind speeds used to calculate gas fluxes for the $MAPCO_2$ drifter use shipboard measurements when the R/V *Ronald H. Brown* was nearby (deployment 1 and deployment 3), and from the QuikSCAT satellite when the ship was not present. Shipboard and QuikSCAT winds are directly compared by *Ho et al.* [2011b]. All wind speeds were interpolated to match the sampling times of the SAMI sensors (Figure 2). At high wind speeds bubble entrainment can have significant impacts on air-sea gas exchange, especially poorly soluble gases such as O_2 and Ar [*Woolf and Thorpe*, 1991]. To assess the *Woolf and Thorpe* [1991] bubble-mediated gas exchange parameterization for this study, we examined mixed layer Ar data (not shown) from discrete, shipboard measurements of O_2/Ar and O_2 concentration during SO GasEx (Hamme et al., submitted manuscript, 2011). Argon and O_2 have similar solubilities and diffusivities, so they respond similarly to bubbles. Using a one-dimensional mixed layer model (see Hamme et al. (submitted manuscript, 2011) for details of the model), we found that diffusive and bubble mediated gas exchange were the dominant processes affecting mixed layer Ar concentrations with entrainment a very minor flux. We found that the observed Ar concentrations could be explained within calculation uncertainty by air-sea gas exchange using the Woolf and Thorpe parameterization for bubbles. Consequently, it was also necessary to use this parameterization to model O_2.

[15] Vertical entrainment fluxes (i.e., mixing), driven by an increase in MLD (H), were calculated from:

$$F_{ent} = \frac{H_i(C_{z_i'} - C_{z_{i-1}})dz}{H_{i-1}\Delta t}, \quad (4)$$

where $C_{z'}$ and C_z indicate concentration of DIC or O_2 of the entrained water and within the ML, respectively, dz is the increase in the MLD, Δt is the time step (1/2 h), and i and i − 1 are the current and previous time steps, respectively. F_{ent} is assumed to be 0 when dz is <=0, as no new water is entrained. The MLD was calculated from the depth-interpolated temperature, which was 18 h low-pass filtered to remove an internal wave present in all of the data (12 h period, see below). A ΔT of 0.3°C (calculated as the difference between the surface T and T at depth) was used to calculate the MLD. This ΔT best matched up with a $\Delta\sigma_\theta$ of 0.01 kg m^{-3} calculated from the CTD profiles and physical model (general ocean turbulence model (GOTM) [*Ho et al.*, 2011a]), a density difference commonly used to define the MLD [*Ho et al.*, 2011a]. Because of an intense rain storm during the third drifter deployment, temperature was not always sufficient to calculate the MLD, and the MLD was calculated from shipboard CTD density profiles. Additionally, based upon the output from the GOTM model [*Ho et al.*, 2011a], the vertical transport across the base of the mixed layer via eddy diffusion is small, and is assumed to be negligible over the length of this study.

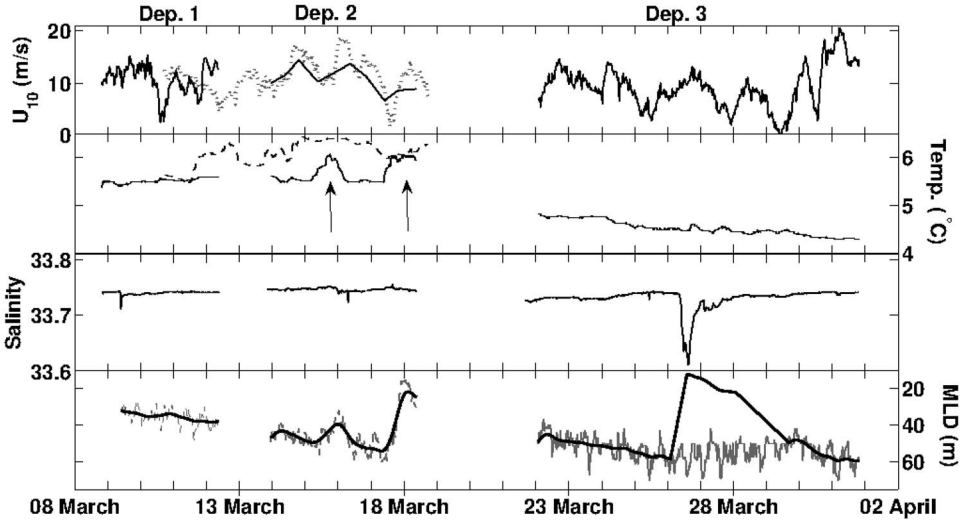

Figure 2. The first panel shows wind speed normalized to 10 m. Solid line indicates combined shipboard and QuickSCAT wind speeds, and dotted line indicates wind speeds from the ASIS drifter. The second panel shows in situ temperature recorded by the 5 m deep SAMI on the $MAPCO_2$ drifter (solid line) and the 1 m deep SAMI on the ASIS drifter (dashed line). Arrows indicate when a neighboring water mass was intruding (higher temperature). The third panel shows salinity recorded by the $MAPCO_2$ drifter. The fourth panel shows MLD calculated from in situ temperature (thin line) and 18 h filtered MLD (heavy line). From 26 to 29 March MLD was estimated based on shipboard CTD density profiles. Gaps indicate when the $MAPCO_2$ drifter was out of the water.

2.6. Calculation Uncertainties

[16] Uncertainties are large when modeling any natural system. Analytical uncertainties for the methods used in this study are small, however, so are the chemical changes observed, thus small uncertainties can cause large errors. Analytical uncertainties in our pCO_2 and O_2 measurements (see above) lead to a ±10% to 50% uncertainty in our air-sea gas fluxes and vertical entrainment fluxes. Methodological errors also contribute to uncertainty in modeling studies. *Ho et al.* [2006] give a 7% uncertainty for their air-sea gas parameterization. *Ho et al.* [2011b] find that the *Ho et al.* [2006] relationship gives an excellent fit with the gas transfer velocities measured during the SO-GasEx cruise and with previous studies. Uncertainty in the calculated MLD can also lead to errors in modeled calculations. An uncertainty in our calculated MLD of ±5 m (the height of the observed internal wave) will give an uncertainty in the depth of the ML of 10% to 20%, which propagates through equations (1) and (4).

3. Results

3.1. Overview

[17] The results presented below are separated into data collected during the three drifter deployments, beginning with the physical data, followed by the chemical data, and then flux and mass balance calculations. A common trend in all of the data was the presence of an internal wave(s), which can be seen in the unfiltered MLD in Figure 2. The three drifter deployments experienced markedly different conditions. Deployment 1 took place during a relatively low wind period, deployment 2 occurred during a storm with wind speeds in excess of 18 m s^{-1}, and during deployment 3 the water mass being observed split following an intense rain storm. The drifter was deployed in an eddy which was bounded to the north by a higher-temperature water mass and to the south by one with a lower temperature (Figure 1).

3.2. Deployment 1

3.2.1. Physical Conditions

[18] During the first $MAPCO_2$ drifter deployment the mean wind speeds were 10.7 ± 2.5 m s^{-1}, sea surface salinity (SSS) averaged 33.740 ± 0.003, and sea surface temperature (SST) averaged 5.52 ± 0.05°C (Figure 2). These small changes in hydrographic conditions reflect the trajectory of the drifter, which appeared to track the surface isotherm closely (Figure 1). The MLD increased from 32 m to 39 m during this 3 day period. When the ASIS drifter was deployed, the SST recorded by it initially matched that of the $MAPCO_2$ drifter, but the ASIS drifter moved away from the tracer patch into warmer waters (Figure 1), where the SST reached a high of 6.28°C.

3.2.2. pCO_2, DIC, and O_2

[19] The location for patch 1 was selected in part because the difference between sea surface and atmospheric pCO_2 was greater than 40 μatm, allowing for direct flux measurements of CO_2 [*McGillis et al.*, 2001]. Initial sea surface pCO_2 was 315 μatm, 66 μatm below the atmospheric level, and gradually increased to a maximum of 323 μatm (Figures 3 and 4). Calculated DIC concentrations increased from 2100 μmol kg^{-1} to 2103 μmol kg^{-1} over the 2.5 day deployment. Surface O_2 concentrations were initially at 319 μmol kg^{-1} and decreased to 315 μmol kg^{-1} by the end of the deployment. The pCO_2, DIC, and O_2

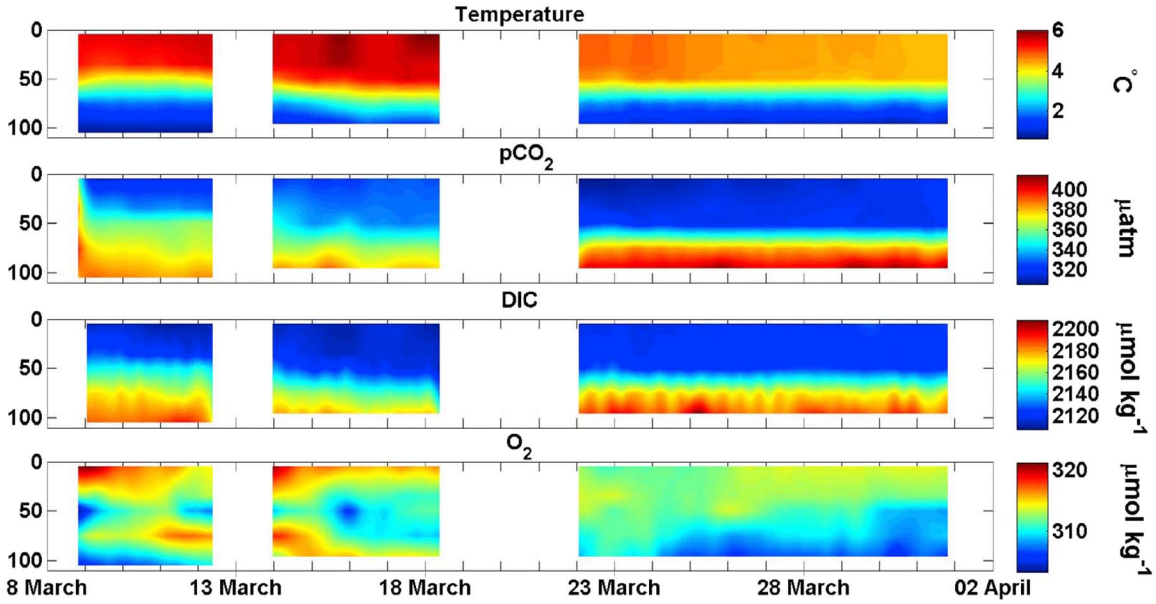

Figure 3. Contour plots of the 18 h filtered temperature, pCO_2, DIC, and O_2 concentrations collected by the SAMI-CO_2 sensors on the MAPCO$_2$ drifter. Gaps indicate when the MAPCO$_2$ drifter was out of the water. Data were filtered to damp the presence of an internal wave.

concentrations exhibit a weak diurnal oscillation, with pCO_2 varying by up to ±5 μatm and DIC and O_2 concentrations varying by ±1 μmol kg^{-1} (Figure 5).

[20] Temperature, pCO_2, and DIC below the MLD remained relatively uniform (Figure 3). Midway through the deployment a slightly higher O_2 water mass was present beneath the mixed layer (Figure 3, 75 m). This change in O_2 concentrations suggests that the surface layer migrated over a deeper water mass with different chemical properties.

3.2.3. Mass Balance

[21] The cumulative change in pCO_2, DIC, and O_2 ($\Sigma H\frac{dC}{dt}$), and the contributions of F_{gasex} (equations (2) and (3)) and F_{ent} (equation (4)) are shown in Figure 5. The surface ocean was a net sink of atmospheric CO_2 and a net source of O_2 (Table 1). Overall, during deployment 1, F_{gasex} accounted for a 2.8 μatm increase in pCO_2, a 1.6 μmol kg^{-1} increase in DIC, and a 3.6 μmol kg^{-1} decrease in O_2 (Figure 5). Correcting for bubble entrainment reduced the change in ML O_2 from F_{gasex} to 0.9 μmol kg^{-1}. The vertical entrainment fluxes were episodic, hence the comparatively rapid increases in F_{ent} followed by a leveling off. F_{ent} was larger than F_{gasex} for pCO_2 and DIC (Table 1), resulting in a 4.7 μatm increase in mixed layer pCO_2, and a 3.0 μmol kg^{-1} increase in DIC. In contrast, F_{ent} was smaller than F_{gasex} for O_2 due to a small vertical gradient, resulting in a 0.9 μmol kg^{-1} decrease in O_2 (Figure 5). Additionally, during this deployment a slight increase in temperature was responsible for a 1.2 μatm increase in pCO_2 (Figure 5). NCP was calculated as the

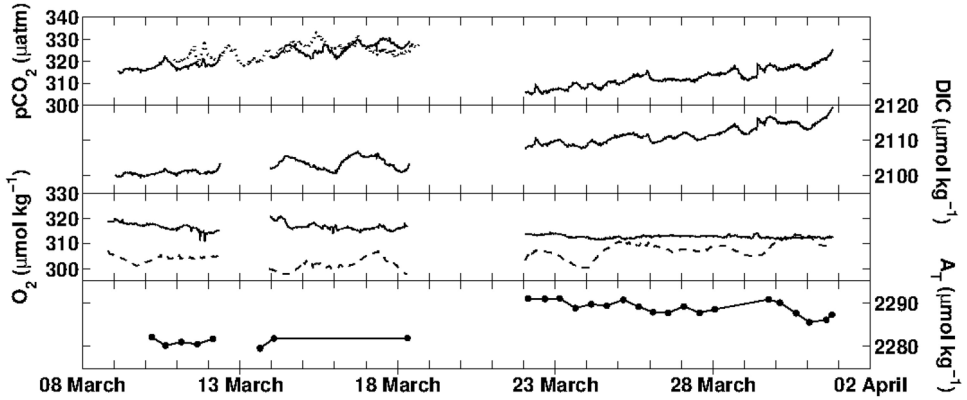

Figure 4. In situ mixed layer pCO_2, DIC, and O_2 from the MAPCO$_2$ drifter and shipboard A_T. Atmospheric pCO_2 recorded by the MAPCO$_2$ sensor on the drifter averaged 381 μatm. The dotted line in the first panel shows the pCO_2 data from the ASIS drifter, and the dashed line in the third panel indicates O_2 saturation at the observed atmospheric pressure.

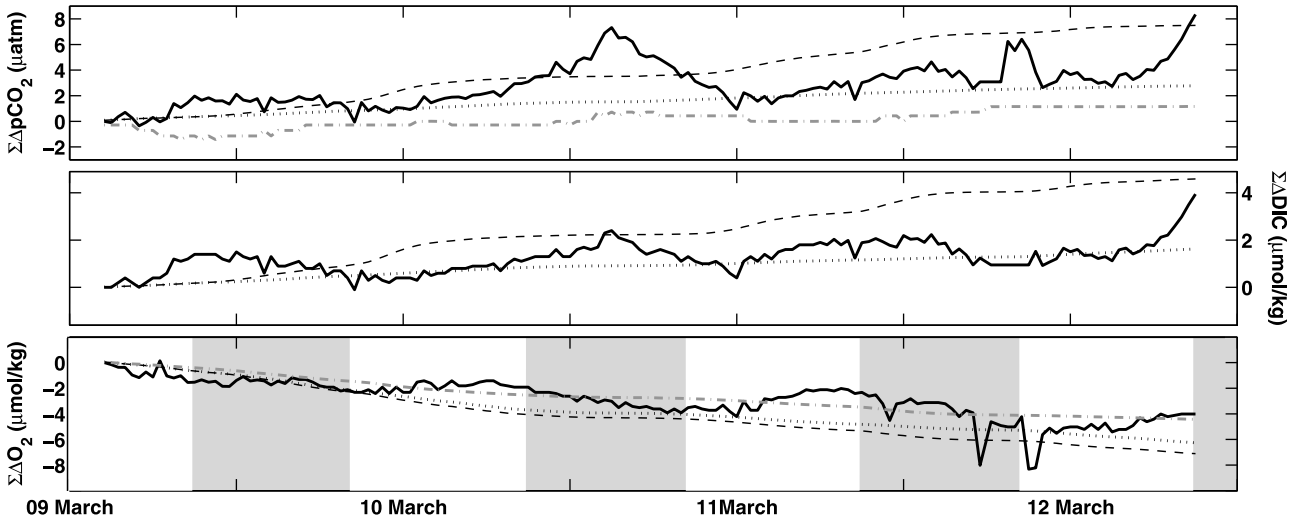

Figure 5. Cumulative measured changes in pCO_2, DIC, and O_2 (solid heavy lines); sum of the total change due to F_{gasex} (dotted lines); sum of the total change due to $F_{gasex} + F_{ent}$ (dashed lines); and bubble entrainment corrected O_2 $F_{gasex} + F_{ent}$ (heavy grey dash-dotted line in the third panel) during the first deployment. Changes in pCO_2 due to temperature are indicated by the heavy grey dot-dashed line (first panel). The grey bars in the third panel indicate nighttime.

residual of the mass balance calculations (equation (1)). NCP for DIC and O_2 averaged 6.7 ± 9.2 and 3.2 ± 9.9 mmol C m^{-2} d^{-1}, respectively (Table 1; O_2 NCP fluxes are reported in C units for ease of comparison, and positive NCP fluxes indicate biological uptake). The NCP calculated from DIC and O_2 are the same within the uncertainty of the mass balance.

3.3. Deployment 2

3.3.1. Physical Conditions

[22] The second deployment of the MAPCO$_2$ drifter provides a contrast to the relatively stable conditions seen in the first deployment. Wind speeds averaged 12.2 ± 3.5 m s^{-1}, reaching a maximum of 18.7 m s^{-1} midway through the deployment and a low of 1.9 m s^{-1} near the end of the deployment (Figure 2). The SSS remained nearly constant, averaging 33.747 ± 0.003. SST was more variable, averaging 5.67 ± 0.21°C, and twice reached maxima in excess of 6°C (Figure 2, arrows in second panel). The increases in SST appear to correlate (not shown, R = 0.69, p value < 0.05) with times when the wind direction recorded by the ASIS drifter (which was used due to the sparse QuickSCAT data) switched from westerly to northerly on 15 and 18 March (Figure 6), and the increase in temperature was seen down to depths of 35 m (Figure 3). A similar correlation is seen in the DIC data (R = 0.63, p value < 0.05). The ASIS drifter also appears to have migrated into a neighboring water mass (Figure 1), and the temperature maxima recorded by the 5 m SAMI-CO_2 were similar to the SST recorded by the ASIS drifter (Figure 2). The MLD, initially at 45 m, deepened to 55 m (Figure 2). During the two SST maxima, the MLD shoaled up to 40 and 23 m. The correlation between DIC, SST, and wind direction suggests that when the winds were out of the north a neighboring water mass intruded upon our study site. The MLD depth shoaled up when the intruding water mass was present, so most of the drogues were below the surface mixed layer (drogue depth ranged from 25 to 91 m), and the drifter likely was not tracking the surface water mass. The ship was not present during a significant portion of this deployment and therefore no samples were taken to establish the location of the patch.

3.3.2. pCO_2, DIC, and O_2

[23] Initial ML pCO_2 in the second deployment was 322 μatm which increased to 329 μatm by the end of the deployment (Figure 4). DIC shows little overall change, increasing by only 1 μmol kg^{-1} from an initial concentration of 2102 μmol kg^{-1}. There is no obvious diurnal cycle present in the DIC data, instead DIC varies by up to 7 μmol kg^{-1} with SST. As was stated above, DIC was significantly correlated with wind direction (Figure 6), with lower DIC concentrations occurring when the winds

Table 1. Average Mixed Layer DIC and O_2 Fluxes for Each Deployment Calculated From Equations (2)–(4)[a]

	Deployment		
	1	2	3
$H\frac{dC}{dt}$			
DIC	43.8	11.0	53.8
O_2	−44.7	−39.2	6.3
F_{gasex}			
DIC	17.8	16.2	17.5
O_2	−39.4 (−69.3)	−55.7 (−82.6)	8.5 (−18.3)
F_{ent}			
DIC	32.7	35.8	29.0
O_2	−9.5	−28.9	−7.0
NCP			
DIC	6.7	nc	−7.3
O_2	3.2 (25.6)	nc	−5.2 (16.0)

[a]All fluxes have units of mmol m^{-2} d^{-1}. O_2 F_{gasex} and NCP values in parentheses have not been corrected for bubble entrainment [*Woolf and Thorpe*, 1991] and are included for comparison. NCP is given in C units for O_2 for ease of comparison. During the second deployment NCP was not calculated (nc) due to interference from an intruding water mass.

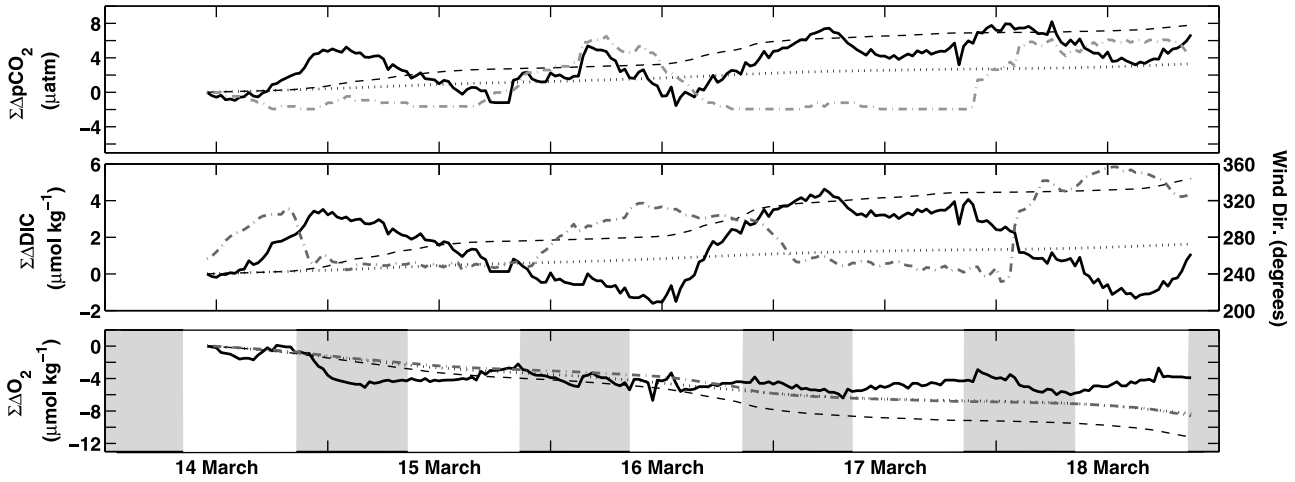

Figure 6. Cumulative measured changes in pCO_2, DIC, and O_2 (solid heavy lines); sum of the total change due to F_{gasex} (dotted lines); sum of the total change due to $F_{gasex} + F_{ent}$ (dashed lines); and bubble entrainment corrected O_2 $F_{gasex} + F_{ent}$ (heavy grey dash-dotted line in the third panel) during the second deployment. Changes in pCO_2 due to temperature are indicated by the heavy grey dot-dashed line (first panel). The gray bars in the third panel indicate nighttime. Bubble entrainment corrected O_2 $F_{gasex} + F_{ent}$ falls on the F_{ent} line during this deployment. The large changes in DIC are due to the intrusion of a neighboring water mass driven by changes in wind direction (heavy dot-dashed line in the second panel), which can also be seen in the temperature increase at the same time in Figures 2 and 3.

were out of the north, and higher DIC concentrations (comparable to those observed during the first deployment) when the winds were out of the west.

[24] The pCO_2 observed by the ASIS drifter were within 10 μatm of those observed by the $MAPCO_2$ drifter (Figure 4, see caption). While no A_T data are available for the intruding water mass, the SSS was similar, so DIC data calculated during this deployment are likely accurate. Since the SST of the intruding water mass was higher, and the pCO_2 was similar to that observed in the patch, the DIC of the intruding water was lower (Figure 4). In contrast to DIC, O_2 was not correlated with wind direction, and instead a small diurnal signal is present (Figure 6). From this it appears that the intruding water mass had similar O_2 characteristics as the $MAPCO_2$ water mass. During the second deployment temperature below the MLD remained constant, however, the high O_2 water mass at 75 m seen in the first deployment sank below our deepest sensor (96 m) at the time of the first temperature maxima (Figure 3).

3.3.3. Mass Balance

[25] The cumulative changes in pCO_2, DIC, and O_2 are markedly different, with the changes in DIC and pCO_2 being dominated by the intrusion of the neighboring water mass while O_2 was relatively constant (Figure 6). As was the case in the first deployment, the surface ocean was always a sink for atmospheric CO_2 and a source of O_2 (Table 1), and F_{gasex} resulted in a 3.3 μatm increase in pCO_2, a 1.6 μmol kg^{-1} increase in DIC, and a 5.7 μmol kg^{-1} decrease in O_2. During this deployment correcting O_2 for bubble entrainment reduced the change in ML O_2 due to F_{gasex} to 3.1 μmol kg^{-1}. The MLD, even though it shoaled up twice during this deployment, had a net increase of 10 m, and F_{ent} caused the mixed layer pCO_2 to increase by 4.5 μatm, DIC to increase by 3.6 μmol kg^{-1}, and O_2 to decrease by 2.9 μmol kg^{-1}. NCP was not calculated for this deployment, as we have insufficient data to account for lateral advection.

3.4. Deployment 3

3.4.1. Physical Conditions

[26] Following the storm the $MAPCO_2$ and ASIS drifters were recovered, and the $MAPCO_2$ drifter was redeployed in a new $^3He/SF_6$ tracer patch on 22 March (Figure 1). Wind speeds in the third deployment ranged from 0.1 to 20.5 m s^{-1}, with a mean of 9.2 ± 4.0 m s^{-1} (Figure 2). Throughout deployment 3 the temperature in the mixed layer decreased, from an initial temperature of 5.0°C to a final temperature of 4.3°C (Figures 2 and 3). The mean sea surface salinity was 33.731 ± 0.018, and it reached a low of 33.612 following a rain storm on 26 March (Figure 2), after which tracer patch 2 split and the $MAPCO_2$ drifter moved away from the main tracer patch which was followed by the ship. However, significant tracer was also found at the location where the drifter was recovered. At the point of divergence of the drifter and patch, the drifter moved south crossing isotherms into colder water (Figure 1). The MLD was steadily increasing prior to the rain storm, from a minimum of 45 m at the beginning of the deployment to 58 m at the beginning of the rain event. The rain storm caused the MLD to rapidly shoal up to 12 m, after which it gradually increased to 59 m.

3.4.2. pCO_2, DIC, and O_2

[27] The mixed layer pCO_2 was initially lower than in the first 2 deployments, as the drifter was deployed in a new water mass, and increased by 20 μatm from 305 to 325 μatm during the deployment (Figure 4). In contrast, DIC concentrations were higher (Figure 4), as A_T was higher, and DIC increased by 10 μmol kg^{-1} from an initial concentration of 2108 μmol kg^{-1}. O_2 concentrations oscillated slightly

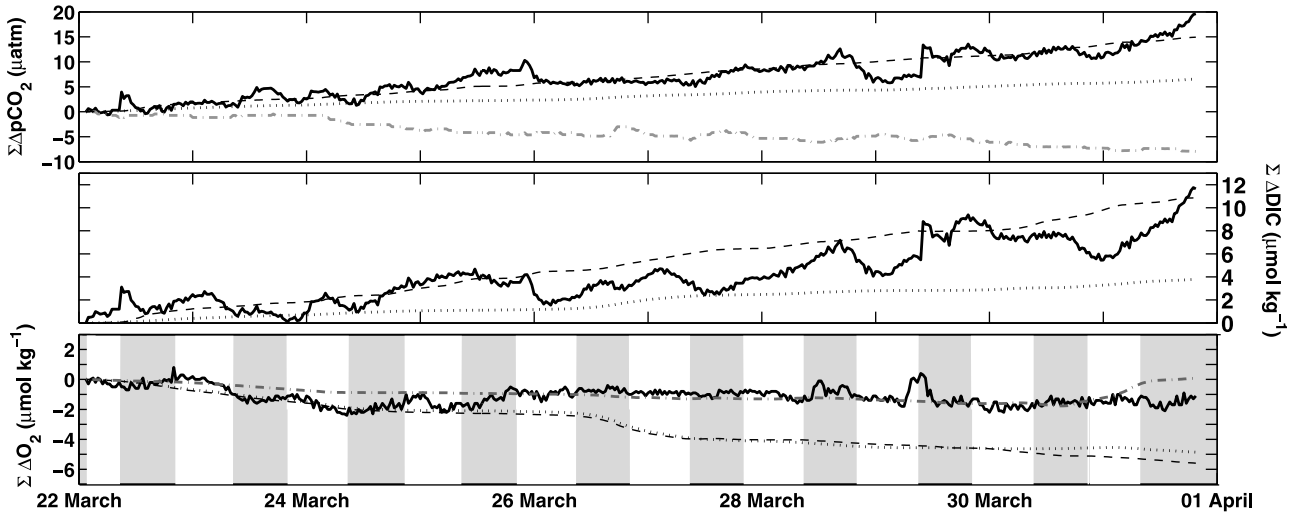

Figure 7. Cumulative measured changes in pCO_2, DIC, and O_2 (solid heavy lines); sum of the total change due to F_{gasex} (dotted lines); sum of the total change due to $F_{gasex} + F_{ent}$ (dashed lines); and bubble entrainment corrected O_2 $F_{gasex} + F_{ent}$ (heavy grey dash-dotted line in the third panel) during the third deployment. Changes in pCO_2 due to temperature are indicated by the heavy grey dot-dashed line (first panel). Changes in pCO_2 due to temperature are indicated by the heavy grey dot-dashed line. The grey bars in the third panel indicate nighttime.

above saturation (Figure 7), decreasing by 0.9 μmol kg^{-1} from an initial concentration of 313.7 μmol kg^{-1}.

3.4.3. Mass Balance

[28] As was the case with the other 2 deployments, the ocean was a net sink of CO_2. Dissolved O_2, however, was at or near saturation throughout this deployment. The average F_{gasex} for pCO_2 and DIC are higher than those observed during the first deployment (Table 1), and F_{gasex} for O_2 was much lower. F_{gasex} resulted in a 6.6 μatm increase in pCO_2, a 3.1 μmol kg^{-1} increase in DIC, and a 0.8 μmol kg^{-1} increase in O_2 after correction for bubble entrainment (Figure 7). Correcting O_2 for bubble entrainment reduced the change in ML O_2 due to F_{gasex} by 3.8 μmol kg^{-1}. The 14 m increase in MLD was larger than that seen in the previous 2 deployments; however, this occurred over a longer time period and, as a result, the average F_{ent} during the third deployment was lower than previously observed (Table 1). Overall, F_{ent} was responsible for a 8.4 μatm increase in pCO_2, a 6.9 μmol kg^{-1} increase in DIC, and a 2.8 μmol kg^{-1} decrease in O_2. Temperature during this deployment decreased by 0.7°C, which resulted in a 9 μatm decrease in pCO_2. Based on both the DIC and O_2 mass balances, NCP during the third deployment was net heterotrophic, and the NCP calculated from DIC and O_2 are the same within calculation uncertainties (-7.3 ± 8.4 mmol C m^{-2} d^{-1} for DIC and -5.2 ± 6.7 mmol C m^{-2} d^{-1} for O_2).

4. Discussion

4.1. Comparison of the Three Deployments

[29] During all 3 deployments the fluxes of CO_2 due to air-sea gas exchange were similar, however, the relative amount they contributed to the ML carbon budget was markedly different. The F_{ent} during deployment 1 for DIC was 1.8 times greater than F_{gasex} (Table 1). For O_2, F_{gasex} was 4.1 times greater than F_{ent}, and during deployment 2 F_{ent} was 2.2 greater than F_{gasex}. F_{ent} for O_2 was almost 2 times greater than the first deployment, and F_{gasex} was 1.9 times greater than F_{ent}. During the third deployment, which was in a new water mass, conditions were different. F_{ent} for DIC was 1.3 times greater than F_{gasex}. O_2 was near saturation most of the deployment (within analytical uncertainty), thus the net O_2 sink during this deployment should be regarded with care. The magnitude of F_{ent} for O_2 was smaller than that observed during the previous deployments. NCP during deployment 1 offset 15% of the DIC increase and 10% of the O_2 decrease, and during the third deployment, which was in a different water mass, NCP was not a significant contributor. Overall, during the first 2 deployments mixed layer CO_2 fluxes were primarily controlled by vertical entrainment, while during the third deployment vertical entrainment fluxes and gas exchange fluxes were nearly equal. Gas exchange fluxes were generally much greater than vertical entrainment for O_2. Additionally, correcting the O_2 air-gas exchange rates for bubble entrainment reduced the fluxes by a factor of 1.4 to 1.6 for the three deployments. Thus it is apparent that no single process dominated the changes in the ML DIC and O_2 budgets, and knowledge of air-sea gas exchange, vertical entrainment, and less so biological processes are necessary to understand this system over this month long study.

[30] During periods when they overlap, our NCP results fall within the range of rates from other studies conducted during the SO-GasEx cruise. *Lee et al.* [2011] found that ^{15}N new productivity averaged ~11 mmol C m^{-2} d^{-1} during the first deployment and ~3.5 mmol C m^{-2} d^{-1} during the third deployment. Hamme et al. (submitted manuscript, 2011) present a comprehensive review of the NCP calculations performed during the SO-GasEx cruise, and our results agree reasonably well with the values presented there. During the first drifter deployment they report NCP values of 7 to 17 mmol C m^{-2} d^{-1}, depending on the method

used, and during the third deployment they report values of 13 to −50 mmol C m^{-2} d^{-1}.

4.2. Comparison With Previous Studies

[31] Southern Ocean data from the CDIAC/WOCE database (http://cdiac.ornl.gov) in similar areas (just south of the PF) have similar pCO_2 (340 μatm), DIC (2120 μmol kg^{-1}), and A_T (2280 μmol kg^{-1}) as those observed within the mixed layer during this study (Figure 4). Air-sea gas fluxes calculated in this study are comparable to those calculated by *Takahashi et al.* [2009] (16.2 to 17.8 mmol C m^{-2} d^{-1} in this study as compared to 6.7 to 12.3 mol C m^{-2} d^{-1}). *Fransson et al.* [2004a, 2004b] found that the southern Atlantic Ocean near the PF was a weak source of atmospheric CO_2 and a sink for O_2 during the austral winter of 1997–1998. A biogeochemical model by *Metzl et al.* [2006] calculated a pCO_2 in March of ~320 μatm in this region, increasing to 340 μatm by April, similar to the changes in pCO_2 observed in this study. The low pCO_2 seen at this time is attributed to residual summer primary productivity as summer transitions to winter, and pCO_2 begins to increase due to entrainment of CO_2 rich waters and gas exchange [*Metzl et al.*, 2006].

[32] As stated above, few detailed studies have been conducted on individual patches of water in the Southern Ocean, and most of those have been performed as control studies during iron fertilization experiments. The first Southern Ocean iron fertilization study, SOIREE [*Boyd et al.*, 2000], took place in February 1999, within the ACC between 60 and 61°S in the Pacific sector of the Southern Ocean. During the 13 days of this study, pCO_2, DIC, and chlorophyll *a* outside of the iron fertilization patch remained relatively constant, with a small net air-sea CO_2 flux into the patch. In November 2000, a second iron fertilization study was conducted in the Southern Ocean at 48°S in the Atlantic sector, within the ACC (EisenEx [*Bozec et al.*, 2005]). Over the 21 day experiment of this study the pCO_2 in waters outside of the iron fertilization patch remained at equilibrium with the atmosphere (362 μatm), and DIC outside the patch remained near 2130 μmol kg^{-1}. The Southern Ocean iron exchange study, SOFeX, was conducted during January and February 2002 [*Coale et al.*, 2004; *Hiscock and Millero*, 2005]. During SOFeX 2 iron fertilization patches were created, a northern patch at 56°S within the ACC and a southern patch at 66°S (both within the Pacific sector), south of the ACC. The northern patch was in waters similar to those in this study (south of the PF, within the ACC). Over the course of the 33 day study nutrient concentrations remained constant in the waters outside the northern iron enrichment site, DIC decreased by 15 μmol kg^{-1}, and pCO_2 increased by 5 μatm, however; no explanation was given for these changes. As was noted in the introduction, primary production rates in unaltered water masses were 11–17 mmol C m^{-2} d^{-1}, which are comparable to our NCP fluxes from the first deployment (Table 1). During the SOFeX study Lagrangian profilers were deployed inside and outside of the iron fertilization patches, and were allowed to drift free for over a year after the study [*Bishop et al.*, 2004; *Bishop*, 2009]. During the austral fall these profilers recorded minimal POC fluxes near the PF, which agree with the low NCP observed in this study.

[33] This study documents a number of the processes controlling mixed layer DIC and O_2 concentrations near the PF in the Southern Ocean. The relative magnitude of the air-sea gas exchange and vertical entrainment fluxes, as compared to the biological fluxes, show that during the austral fall mixed layer DIC and O_2 concentrations are primarily controlled by physical processes. However, as was shown above, the Southern Ocean is highly heterogeneous, making accurate quantification of seasonal and annual CO_2 fluxes difficult. Long-term, basin-wide measurements of pCO_2 and other biogeochemical parameters are needed to more accurately address the role the Southern Ocean plays in the global carbon cycle.

[34] **Acknowledgments.** We thank Cory Beatty (University of Montana) for technical support and the Captain and crew of the NOAA R/V *Ronald H. Brown* for cruise logistics. We would also like to thank the four anonymous reviewers for their thoughtful comments. NSF (OCE-0726784) and NOAA (NA07OAR4310122) funded this research.

References

Bakker, D. C. E., H. J. W. DeBaar, and U. V. Bathmann (1997), Changes of carbon dioxide in surface waters during spring in the Southern Ocean, *Deep Sea Res., Part II*, *44*(1–2), 91–127, doi:10.1016/S0967-0645(96)00075-6.

Bakker, D. C. E., J. Etcheto, J. Boutin, and L. Merlivat (2001), Variability of surface water fCO_2 during seasonal upwelling in the equatorial Atlantic Ocean as observed by a drifting buoy, *J. Geophys. Res.*, *106*(C5), 9241–9253,doi:10.1029/1999JC000275.

Balch, W. M., D. T. Drapeau, B. C. Bowler, E. Lyczskowski, E. S. Booth, and D. Alley (2011), The contribution of coccolithophores to the optical and inorganic carbon budgets during the Southern Ocean Gas Exchange Experiment: New evidence in support of the "Great Calcite Belt" hypothesis, *J. Geophys. Res.*, *116*, C00F06, doi:10.1029/2011JC006941.

Barbero, L., J. Boutin, L. Merlivat, N. Martin, T. Takahashi, S. C. Sutherland, and R. Wanninkhof (2011), Importance of water mass formation regions for the air-sea CO_2 flux estimate in the Southern Ocean, *Global Biogeochem. Cycles*, *25*, GB1005, doi:10.1029/2010GB003818.

Bishop, J. K. B. (2009), Autonomous observations of the ocean biological carbon pump, *Oceanography*, *22*(2), 182–193.

Bishop, J. K. B., T. J. Wood, R. E. Davis, and J. T. Sherman (2004), Robotic observations of enhanced carbon biomass and export at 55°S during SOFeX, *Science*, *304*(5669), 417–420, doi:10.1126/science.1087717.

Boning, C. W., A. Dispert, M. Visbeck, S. R. Rintoul, and F. U. Schwarzkopf (2008), The response of the Antarctic Circumpolar Current to recent climate change, *Nat. Geosci.*, *1*(12), 864–869, doi:10.1038/ngeo362.

Boyd, P. W., et al. (2000), A mesoscale phytoplankton bloom in the polar Southern Ocean stimulated by iron fertilization, *Nature*, *407*(6805), 695–702, doi:10.1038/35037500.

Bozec, Y., D. C. E. Bakker, C. Hartmann, H. Thomas, R. G. J. Bellerby, P. D. Nightingale, U. Riebesell, A. J. Watson, and H. J. W. de Baar (2005), The CO_2 system in a Redfield context during an iron enrichment experiment in the Southern Ocean, *Mar. Chem.*, *95*(1–2), 89–105, doi:10.1016/j.marchem.2004.08.004.

Bryden, H. L., and S. A. Cunningham (2003), How wind-forcing and air-sea heat exchange determine the meridional temperature gradient and stratification for the Antarctic Circumpolar Current, *J. Geophys. Res.*, *108*(C8), 3275, doi:10.1029/2001JC001296.

Coale, K. H., et al. (2004), Southern Ocean Iron Enrichment Experiment: Carbon cycling in high- and low-Si waters, *Science*, *304*(5669), 408–414, doi:10.1126/science.1089778.

de Baar, H. J. W., J. T. M. de Jong, R. F. Nolting, K. R. Timmermans, M. A. van Leeuwe, U. Bathmann, M. R. van der Loeff, and J. Sildam (1999), Low dissolved Fe and the absence of diatom blooms in remote Pacific waters of the Southern Ocean, *Mar. Chem.*, *66*(1–2), 1–34, doi:10.1016/S0304-4203(99)00022-5.

DeGrandpre, M. D., T. R. Hammar, S. P. Smith, and F. L. Sayles (1995), In-situ measurements of seawater pCO_2, *Limnol. Oceanogr.*, *40*(5), 969–975.

DeGrandpre, M. D., R. Wanninkhof, W. R. McGillis, and P. G. Strutton (2004), A Lagrangian study of surface pCO_2 dynamics in the eastern equatorial Pacific Ocean, *J. Geophys. Res.*, *109*, C08S07, doi:10.1029/2003JC002089.

Dickson, A., and F. Millero (1987), A comparison of the equilibrium constants for the dissociation of carbonic acid in seawater media, *Deep Sea Res., Part A*, *34*(10), 1733–1743, doi:10.1016/0198-0149(87)90021-5.

Dickson, A. G., J. D. Afghan, and G. C. Anderson (2003), Reference materials for oceanic CO_2 analysis: A method for the certification of total alkalinity, *Mar. Chem.*, *80*(2–3), 185–197, doi:10.1016/S0304-4203(02)00133-0.

Donelan, M. (1990), Air-sea interaction, in *The Sea: Ocean Engineering Science*, vol. 9, pp. 241–292, John Wiley, New York.

Fletcher, S., et al. (2006), Inverse estimates of anthropogenic CO_2 uptake, transport, and storage by the ocean, *Global Biogeochem. Cycles*, *20*, GB2002, doi:10.1029/2005GB002530.

Fransson, A., M. Chierici, and L. G. Anderson (2004a), Diurnal variability in the oceanic carbon dioxide system and oxygen in the Southern Ocean surface water, *Deep Sea Res., Part II*, *51*(22–24), 2827–2839, doi:10.1016/j.dsr2.2001.01.001.

Fransson, A., M. Chierici, L. G. Anderson, and R. David (2004b), Transformation of carbon and oxygen in the surface layer of the eastern Atlantic sector of the Southern Ocean, *Deep Sea Res., Part II*, *51*(22–24), 2757–2772, doi:10.1016/j.dsr2.2001.12.001.

Friederich, G. E., P. M. Walz, M. G. Burczynski, and F. P. Chavez (1995), Inorganic carbon in the central California upwelling system during the 1997–1999 El Niño–La Niña event, *Prog. Oceanogr.*, *54*(1–4), 185–203, doi:10.1016/S0079-6611(02)00049-6.

Fyfe, J. C., and O. A. Saenko (2005), Human-induced change in the Antarctic Circumpolar Current, *J. Clim.*, *18*(15), 3068–3073, doi:10.1175/JCLI3447.1.

Garcia, H. E., and L. I. Gordon (1992), Oxygen solubility in seawater: Better fitting equations, *Limnol. Oceanogr.*, *37*, 1307–1312.

Gervais, F., U. Riebesell, and M. Y. Gorbunov (2002), Changes in primary productivity and chlorophyll a in response to iron fertilization in the Southern Polar Frontal Zone, *Limnol. Oceanogr.*, *47*(5), 1324–1335, doi:10.4319/lo.2002.47.5.1324.

Graber, H. C., E. A. Terray, M. A. Donelan, W. M. Drennan, J. C. Van Leer, and D. B. Peters (2000), ASIS—A new air-sea interaction spar buoy: Design and performance at sea, *J. Atmos. Oceanic Technol.*, *17*(5), 708–720, doi:10.1175/1520-0426(2000)017<0708:AANASI>2.0.CO;2.

Guéguen, C., and P. D. Tortell (2008), High-resolution measurement of Southern Ocean CO_2 and O_2/Ar by membrane inlet mass spectrometry, *Mar. Chem.*, *108*(3–4), 184–194, doi:10.1016/j.marchem.2007.11.007.

Hall, A., and M. Visbeck (2002), Synchronous variability in the Southern Hemisphere atmosphere, sea ice, and ocean resulting from the annular mode, *J. Clim.*, *15*(21), 3043–3057, doi:10.1175/1520-0442(2002)015<3043:SVITSH>2.0.CO;2.

Hiscock, W. T., and F. J. Millero (2005), Nutrient and carbon parameters during the Southern Ocean iron experiment (SOFeX), *Deep Sea Res., Part I*, *52*(11), 2086–2108, doi:10.1016/j.dsr.2005.06.010.

Ho, D. T., C. S. Law, M. J. Smith, P. Schlosser, M. Harvey, and P. Hill (2006), Measurements of air-sea gas exchange at high wind speeds in the Southern Ocean: Implications for global parameterizations, *Geophys. Res. Lett.*, *33*, L16611, doi:10.1029/2006GL026817.

Ho, D. T., C. L. Sabine, D. Hebert, D. S. Ullman, R. Wanninkhof, R. C. Hamme, P. G. Strutton, B. Hales, J. B. Edson, and B. R. Hargreaves (2011a), Southern Ocean Gas Exchange Experiment: Setting the stage, *J. Geophys. Res.*, *116*, C00F08, doi:10.1029/2010JC006852.

Ho, D. T., R. Wanninkhof, D. Ullman, D. Hebert, P. Schlosser, and K. Sullivan (2011b), Towards a universal relationship between wind speed and gas exchange: Gas transfer velocities measured with $^3He/SF_6$ during the Southern Ocean Gas Exchange Experiment, *J. Geophys. Res.*, *116*, C00F04, doi:10.1029/2010JC006854.

Hood, E. M., L. Merlivat, and T. Johannessen (1999), Variations of fCO_2 and air-sea flux of CO_2 in the Greenland Sea gyre using high-frequency time series data from CARIOCA drift buoys, *J. Geophys. Res.*, *104*(C9), 20,571–20,584, doi:10.1029/1999JC900130.

Hood, E. M., R. Wanninkhof, and L. Merlivat (2001), Short timescale variations of fCO_2 in a North Atlantic warm-core eddy: Results from the Gas-Ex 98 carbon interface ocean atmosphere (CARIOCA) buoy data, *J. Geophys. Res.*, *106*(C2), 2561–2572, doi:10.1029/1999JC000278.

Johnson, K. M., A. E. King, and J. M. Sieburth (1985), Coulometric TCO_2 analyses for marine studies: An introduction, *Mar. Chem.*, *16*(1), 61–82, doi:10.1016/0304-4203(85)90028-3.

Juranek, L. W., R. C. Hamme, J. Kaiser, R. Wanninkhof, and P. D. Quay (2010), Evidence of O_2 consumption in underway seawater lines: Implications for air-sea O_2 and CO_2 fluxes, *Geophys. Res. Lett.*, *37*, L01601, doi:10.1029/2009GL040423.

Khatiwala, S., F. Primeau, and T. Hall (2009), Reconstruction of the history of anthropogenic CO_2 concentrations in the ocean, *Nature*, *462*(19), 346–349, doi:10.1038/nature08526.

Lee, Z., et al. (2011), An assessment of optical properties and primary production derived from remote sensing in the Southern Ocean (SO GasEx), *J. Geophys. Res.*, *116*, C00F03, doi:10.1029/2010JC006747.

Lenton, A., and R. J. Matear (2007), Role of the Southern Annular Mode (SAM) in Southern Ocean CO_2 uptake, *Global Biogeochem. Cycles*, *21*, GB2016, doi:10.1029/2006GB002714.

Le Quéré, C., T. Takahashi, E. T. Buitenhuis, C. Rodenbeck, and S. C. Sutherland (2010), Impact of climate change and variability on the global oceanic sink of CO_2, *Global Biogeochem. Cycles*, *24*, GB4007, doi:10.1029/2009GB003599.

Lovenduski, N. S., N. Gruber, and S. C. Doney (2008), Toward a mechanistic understanding of the decadal trends in the Southern Ocean carbon sink, *Global Biogeochem. Cycles*, *22*, GB3016, doi:10.1029/2007GB003139.

Marshall, G. J. (2003), Trends in the Southern Annular Mode from observations and reanalyses, *J. Clim.*, *16*(24), 4134–4143, doi:10.1175/1520-0442(2003)016<4134:TITSAM>2.0.CO;2.

Martin, J. H., R. M. Gordon, and S. E. Fitzwater (1990), Iron in Antarctic waters, *Nature*, *345*(6271), 156–158, doi:10.1038/345156a0.

McGillis, W. R., J. B. Edson, J. E. Hare, and C. W. Fairall (2001), Direct covariance air-sea CO_2 fluxes, *J. Geophys. Res.*, *106*(C8), 729–745, doi:10.1029/2000JC000506.

McNeil, B. I., N. Metzl, R. M. Key, R. J. Matear, and A. Corbiere (2007), An empirical estimate of the Southern Ocean air-sea CO_2 flux, *Global Biogeochem. Cycles*, *21*, GB3011, doi:10.1029/2007GB002991.

Mehrbach, C., C. Culberson, J. E. Hawley, and R. Pytkowiz (1973), Measurement of apparent dissociation-constants of carbonic-acid in seawater at atmospheric-pressure, *Limnol. Oceanogr.*, *18*(6), 897–907.

Merlivat, L., M. Gonzalez Davila, G. Caniaux, J. Boutin, and G. Reverdin (2009), Mesoscale and diel to monthly variability of CO_2 and carbon fluxes at the ocean surface in the northeastern Atlantic, *J. Geophys. Res.*, *114*, C03010, doi:10.1029/2007JC004657.

Metzl, N., C. Brunet, A. Jabaud-Jan, A. Poisson, and B. Schauer (2006), Summer and winter air-sea CO_2 fluxes in the Southern Ocean, *Deep Sea Res., Part I*, *53*(9), 1548–1563, doi:10.1016/j.dsr.2006.07.006.

Oke, P. R., and M. H. England (2004), Oceanic response to changes in the latitude of the Southern Hemisphere subpolar westerly winds, *J. Clim.*, *17*(5), 1040–1054, doi:10.1175/1520-0442(2004)017<1040:ORTCIT>2.0.CO;2.

Olbers, D., and M. Visbeck (2005), A model of the zonally averaged stratification and overturning in the Southern Ocean, *J. Phys. Oceanogr.*, *35*, 1190–1205, doi:10.1175/JPO2750.1.

Pierrot, D., E. Lewis, and D. Wallace (2006), MS Excel program developed for CO_2 system calculations, *Tech. Rep., ORNL/CDIAC-105a*, Carbon Dioxide Inf. Anal. Cent., Oak Ridge Natl. Lab., U.S. Dep. of Energy, Oak Ridge, Tenn.

Pierrot, D., C. Neill, K. Sullivan, R. Castle, R. Wanninkhof, H. Luger, T. Johannessen, A. Olson, R. A. Feely, and C. E. Cosca (2009), Recommendations for autonomous underway pCO_2 measuring systems and data-reduction routines, *Deep Sea Res., Part II*, *56*(8–10), 512–522, doi:10.1016/j.dsr2.2008.12.005.

Quéguiner, B., P. Treguer, I. Peeken, and R. Scharek (1997), Biogeochemical dynamics and the silicon cycle in the Atlantic sector of the Southern Ocean during austral spring 1992, *Deep Sea Res., Part II*, *44*(1–2), 69–89, doi:10.1016/S0967-0645(96)00066-5.

Sabine, C. L., et al. (2004), The oceanic sink for anthropogenic CO_2, *Science*, *305*(5682), 367–371, doi:10.1126/science.1097403.

Saenko, O. A. (2008), Influence of the enhanced mixing within the Southern Ocean fronts on the overturning circulation, *Geophys. Res. Lett.*, *35*, L09602, doi:10.1029/2008GL033565.

Shim, J., Y. C. Kang, D. Kim, and S. H. Choi (2006), Distribution of net community production and surface pCO_2 in the Scotia Sea, Antarctica, during austral spring 2001, *Mar. Chem.*, *101*(1–2), 68–84, doi:10.1016/j.marchem.2005.12.007.

Strass, V. H., A. C. N. Garabato, A. U. Bracher, R. T. Pollard, and M. I. Lucas (2002), A 3-D mesoscale map of primary production at the Antarctic Polar Front: Results of a diagnostic model, *Deep Sea Res., Part II*, *49*(18), 3813–3834, doi:10.1016/S0967-0645(02)00112-1.

Takahashi, T., et al. (2009), Climatological mean and decadal change in surface ocean pCO_2, and net sea-air CO_2 flux over the global oceans, *Deep Sea Res., Part II*, *56*(8–10), 554–577, doi:10.1016/j.dsr2.2008.12.009.

Wanninkhof, R. (1992), Relationship between wind-speed and gas-exchange over the ocean, *J. Geophys. Res.*, *97*(C5), 7373–7382, doi:10.1029/92JC00188.

Weiss, R. (1974), Carbon dioxide in water and seawater: The solubility of a non-ideal gas, *Mar. Chem.*, *2*(3), 203–215, doi:10.1016/0304-4203(74)90015-2.

Woolf, D. K., and S. A. Thorpe (1991), Bubbles and the air-sea exchange of gases in near-saturation conditions, *J. Mar. Res.*, *49*, 435–466, doi:10.1357/002224091784995765.

Zhang, J. Z. (2000), Shipboard automated determination of trace concentrations of nitrite and nitrate in oligotrophic water by gas-segmented continuous flow analysis with a liquid waveguide capillary flow cell, *Deep Sea Res., Part I*, *47*(6), 1157–1171, doi:10.1016/S0967-0637(99)00085-0.

Zhang, J. Z., and J. Chi (2002), Automated analysis of nanomolar concentrations of phosphate in natural waters with liquid waveguide, *Environ. Sci. Technol.*, *36*(5), 1048–1053, doi:10.1021/es011094v.

Zickfeld, K., J. C. Fyfe, O. A. Saenko, M. Eby, and A. J. Weaver (2007), Response of the global carbon cycle to human-induced changes in Southern Hemisphere winds, *Geophys. Res. Lett.*, *34*, L12712, doi:10.1029/2006GL028797.

M. D. DeGrandpre and T. S. Moore, Department of Chemistry and Biochemistry, University of Montana, 32 Campus Dr., Missoula, MT 59812, USA. (michael.degrandpre@umontana.edu; tommy.moore@umontana.edu)

W. M. Drennan, Rosenstiel School of Marine and Atmospheric Science, University of Miami, 4600 Rickenbacker Causeway, Miami, FL 33l49, USA. (wdrennan@rsmas.miami.edu)

R. A. Feely and C. L. Sabine, Pacific Marine Environmental Laboratory, 7600 Sand Point Way NE, Seattle, WA 98115, USA. (richard.a.feely@noaa.gov; chris.sabine@noaa.gov)

R. C. Hamme, School of Earth and Ocean Sciences, University of Victoria, Victoria, BC V8W 3P6, Canada. (rhamme@uvic.ca)

W. R. McGillis, Earth and Environmental Engineering, Lamont-Doherty Earth Observatory, Earth Institute at Columbia University, 927 Seely Mudd Bldg., Morningside Campus, New York, NY 10964, USA. (wrm2102@columbia.edu)

C. J. Zappa, Ocean and Climate Physics Division, Lamont-Doherty Earth Observatory, Earth Institute at Columbia University, 206B Oceanography, 61 Rt. 9W, Palisades, NY 10964, USA. (zappa@ldeo.columbia.edu)